

Convection velocity of temperature fluctuations in a natural convection boundary layer

K. M. Talluru, H. F. Pan, K. A. Chauhan and J. Patterson

School of Civil Engineering
The University of Sydney, New South Wales 2006, Australia

Abstract

Simultaneous measurements of temperature are carried out in a thermal boundary layer developing over a vertical hot plate using a combination of an infra-red sensor, three cold wires and a Resistance Temperature device. An aim of this study is to establish experimental procedures for high spatial and temporal resolution temperature measurements. To this end, the growth of thermal boundary layer is documented and compared against existing empirical models. Statistics of mean and fluctuating temperature are in excellent agreement with previously reported experimental data for laminar thermal boundary layers. The thermal boundary layer is observed to grow as $y^{1/2}$, where y is the vertical distance along the heated wall. In addition to this, separate experiments are conducted by varying the heat input to investigate its effect on convection velocity (U_c) of thermal structures in the flow. It is found that U_c remained nominally constant across the boundary layer but increased with Rayleigh number as $Ra^{1/4}$ when heat input is varied.

Introduction

A predominantly vertical flow is generated due to buoyancy force when a heated vertical plate is placed in an ambient space of lower temperature. This phenomenon can be observed in urban areas, where hot air rises next to a concrete wall on a typical summer day. In the recent years, this concept has gained popularity as a passive technique to provide thermal comfort to humans residing within a building, aka *solar chimney*. Despite its merits over forced or fan-driven convective devices, it is quite challenging to predict its performance as the heat transfer rate is governed by the air flow next to the hot vertical plate. The problem is further complicated due to the geometry of ambient space, e.g., a room in a building. This problem has been well studied via experimental [1, 9] and numerical simulation methods [10, 2, and references therein]. Most of the earlier studies treated mainly overall characteristics such as heat transfer, mean temperature and mean velocity profiles [4]. One of the pioneering studies of the turbulence structure of thermal boundary layer was carried out by [6]. This was followed by other studies [7, 8] using a combination of V-shaped hotwires and cold wires to document the fluxes and intensities of velocity and temperature fluctuations. But, none of these studies looked at the evolution of thermal boundary layer in a systematic manner. Further, the space-time correlations of temperature fluctuations have not been well-documented. To this end, we constructed an experimental rig to study the structure of temperature fluctuations in the thermal boundary layer. In particular, the focus of this study is to develop experimental procedures to measure convection velocity of thermal structures that contribute to mass transfer as well as entrainment of ambient fluid into the thermal boundary layer. As a first step towards that goal, here, we discuss results using simultaneous measurements of temperature at three spatially separated points.

Experimental details

Experiments are conducted in a natural convection boundary layer developing over a vertical hot plate whose dimensions are

0.9 m high and 0.3 m wide. A schematic of the experimental setup and instrumentation is shown in figure 1(a). The test rig is built to resemble the essential features of a single-cavity solar chimney. It has a thin aluminium sheet (0.25 mm thickness) painted matt black as the radiative surface. On either side, the rig is covered with glass panels to facilitate optical access. A curved inlet is designed to allow smooth entry of cold air. The hot plate is heated using an artificial light source (Selecon Rama 6" Fresnel theatre lamp), located at a distance of 1 m in front of the test rig. The lamp is powered using an electric transformer to maintain a constant voltage power supply and minimise fluctuations in the heat input to solar chimney. The transformer is also capable of operating the lamp at lower voltages, if required. Although the intensity of radiation from the lamp ($\dot{q} \approx 200 \text{ W/m}^2$) is much less compared to solar radiation that is typically 1000 W/m^2 on a sunny day, it is preferred here as it can maintain steady conditions for a long-duration of time. In the current study, three different power (i.e., 600, 880 and 1200 Watts) settings are used for the lamp. At the highest power setting, a maximum temperature difference of 15°C is noticed between the hot wall and the ambient space. In this configuration, the largest Grashof number ($Gr = g\beta(\Theta_w - \Theta_a)y^3/\nu^2$, where g is gravitational acceleration, β is the coefficient of volumetric expansion, Θ_w and Θ_a are the temperatures of hot wall and the ambient space, respectively) is found to be approximately 5×10^8 and so, the Rayleigh number is 3.5×10^8 , since $Ra = Gr.Pr$ with $Pr = 0.7$ for air. Throughout this paper, x and y respectively refer to coordinates normal and along the vertical hot plate, as shown in the schematic. Also note that, unless specified, the results presented in this paper are obtained when the power output of the lamp is 1200 Watts.

The test rig is instrumented to measure temperature profiles along x at different vertical positions in the cavity. An array of three cold wire sensors (five-micron diameter tungsten wires with probe length of 1.2 mm, operated with constant current anemometers (CCA) from Dantec and TSI, Inc.), is used to measure the time-varying temperature in the thermal boundary layer. Each of the CCA channels have a measurement range of $0\text{-}180^\circ\text{C}$ and a frequency response of 1 kHz. Thus, high spatial and temporal resolution measurements of temperature fluctuations within the thermal boundary layer are possible. The probes are calibrated at five different temperatures between 10°C and 80°C by varying the temperature of a water bath. A linear trend was observed between the measured voltages of cold wires and the temperature. The three CCA probes are mounted on a miniature traverse supplied by Zaber Technologies Inc. that has a resolution of $5 \mu\text{m}$. The vertical spacing between the probes (① and ②) and (② and ③) is 0.02 m and 0.03 m, respectively. Using the traversing system, measurements are acquired at 30 logarithmically spaced points in the horizontal (x) direction and at six different locations in the region, $0.235 \text{ m} \leq y \leq 0.735 \text{ m}$.

A fast response infra-red sensor from Calnex Electronics Ltd. (model PyroCube XS), with a response time of 50 milli-seconds is employed to continuously monitor the surface temperature of the heated plate. The infra-red sensor has a spot size of 1 mm

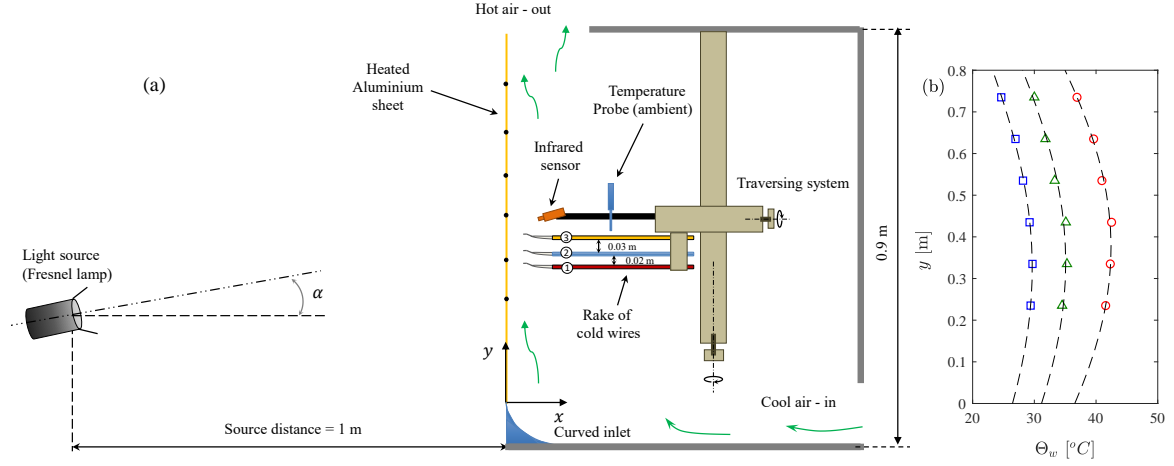


Figure 1: (a) Schematic of solar chimney test rig. (b) Distribution of surface temperatures for three different heat inputs (\circ - 1200 W; \triangle - 880 W; \square - 600 W). The dashed lines show Gaussian curves fitted to the experimental data of wall temperature.

diameter at a focal distance of 100 mm. Thus, local variations of surface temperature over a small area are measured. Although the response time of the infra-red sensor is lower than that of the CCA probe, it provides high spatial resolution for surface temperature that is not achievable with other conventional probes. The infra-red sensor has an overall accuracy of $\pm 0.5^{\circ}\text{C}$ over its set range of $0\text{--}100^{\circ}\text{C}$. The temperature at far end, i.e. at $x = 180\text{ mm}$ is monitored using a resistive temperature device (RTD). Thus any slow variations in ambient conditions are monitored throughout the experiment. These measurements are carried out in a temperature controlled room to maintain steady ambient conditions for the entire duration of the experiment. All the above sensors are simultaneously sampled at a rate of 500 Hz and digitised using a 24-bit resolution Analog-to-Digital card connected to a National Instrument compactDAQ system. Note that capitalised (e.g., Θ) and lower case letters (e.g., θ) indicate mean and fluctuating quantities, while subscripts 'w' and 'a' are used to refer to wall and ambient temperatures, respectively.

Trend of surface temperature

At the start of every experiment, the lamp is turned on for at least 45 minutes to ensure steady conditions in the test rig. During this time, temperature at the wall (Θ_w) is continuously monitored to quantify its transient growth, an example of which is shown in figure 2. It is observed that a combination of two exponential curves is a good fit to the experimental data, which suggests that there are two dominant time scales, $\tau_1 = 1.25\text{ min}$ and $\tau_2 = 16.5\text{ min}$ observed in our study. This type of fit seems plausible considering the fact there is a sharp rise in wall temperature initially indicating smaller time constant (τ_1) and gradual increase of Θ_w (i.e., τ_2) in the later period. This behaviour can be explained by following the approach of [3]. Initially, as the wall is heated by the incident light from the lamp, temperature of the wall rises quickly due to conduction of heat into the fluid. During this time, the buoyancy force or heat transport by convection is weak. But as the temperature rises further, the air present next to the hot wall gets heated leading to vertical convection. At this point, a quasi equilibrium state is established between the conduction of heat into the fluid and convective transport in the vertical direction. Hence, the net rise of wall temperature is slower compared to the start-up region. This is likely to be associated with the larger time constant (τ_2). A comparison of the two time constants indicate that τ_2 is about ten times larger than τ_1 . Looking further, we plotted the variation

of Θ_w along y in figure 1(b) for three different power settings of the lamp. As expected, Θ_w increases with heat input at all locations. More interestingly, for a given power setting, Θ_w has a Gaussian distribution as evident from the excellent agreement (cf. Gaussian curve fits in figure 1(b)). The Gaussian behaviour of wall temperature is due to the parabolic distribution of heat intensity at any cross-section of the light beam emitted by the Fresnel lamp.

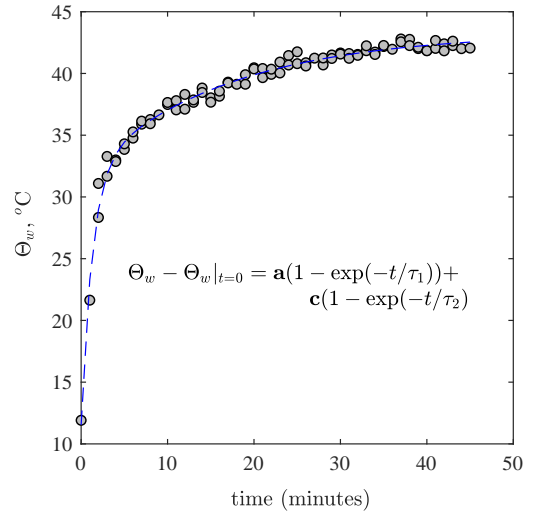


Figure 2: The transient behaviour of wall temperature before reaching a steady state.

Mean and r.m.s profiles of temperature

Figure 3 shows the profiles of normalised mean temperature, $\Theta^* = (\Theta_s - \Theta)/(\Theta_s - \Theta)$ at six different locations along y . Note that the profiles are shifted vertically. As evident, Θ^* has laminar behaviour at all locations, which is due to lower Grashof number in this study. In previous studies [7, 8, 2], it was noticed that Grashof number of at least 10^{10} is required to observe the logarithmic region in the temperature profile. Nonetheless, it is observed that thermal boundary layer is growing along y as illustrated in figure 3. In order to quantify the growth of thermal boundary layer, we calculated the thickness (δ_T) at each measurement location, which is defined as the distance normal to

the hot wall, where $\Theta^* = 0.99$ [5]. The locations corresponding to δ_T are also plotted in figure 3 to facilitate better understanding of the growth of thermal boundary layer. It should be noted that δ_T is computed using a spline interpolation scheme on the experimental data. It is found that δ_T grows as $y^{1/2}$, which is in complete agreement with the analytical expression: $\delta_T = 5.0\sqrt{\frac{\nu y}{u_0}}Pr^{-1/3}$, known for a laminar thermal boundary layer [5]. In the current study, we do not have information of velocity scale u_0 to verify the above relationship, however, the growth of $\delta_T \sim y^{1/2}$ clearly suggests that the flow is laminar. Similar trend of δ_T is observed when the heat output of the lamp is changed to 600 and 880 Watts.

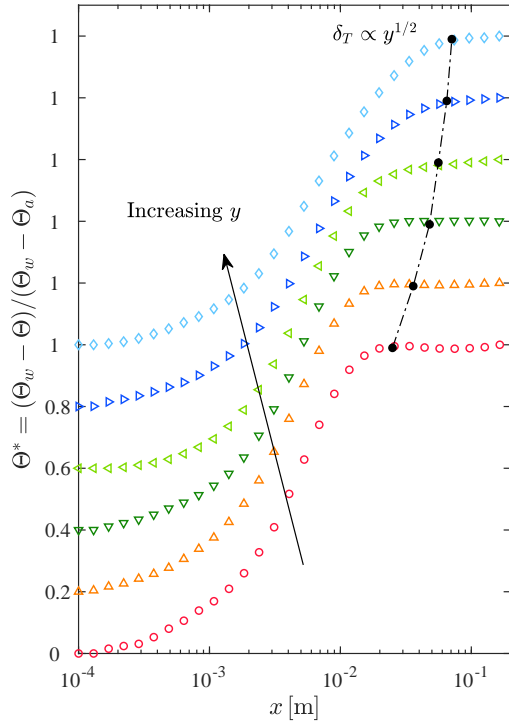


Figure 3: Profiles of $\Theta^* = (\Theta_s - \Theta)/(\Theta_s - \Theta_a)$ in the thermal boundary layer developing along the vertical heated wall. Symbols represent different measurement stations. Note that the profiles are shifted vertically.

As a next logical step, the temperature profiles in figure 3 are replotted in figure 4(a), where the wall-normal distance (x) is normalised by the boundary layer thickness (δ_T). As evident from this figure, the normalised temperature profiles collapse well with an exception at the first measurement station. Two important observations can be made from this figure; first, the normalised temperature profiles are identical across the entire thermal boundary layer and second, there is only one dominant length scale, which is δ_T . This is somewhat anticipated since a laminar flow is governed by a single length scale. The lack of collapse at the first measurement station could be due to the residual effect of the inlet conditions in the test rig. Figure 4(b) shows the normalised root mean square (r.m.s) profiles of temperature fluctuations (expressed as a percentage of $\Theta_w - \Theta_a$) across the thermal boundary layer at different locations along the heated wall. At first, it is easy to see that the r.m.s values increase as the thermal boundary layer grows along y , which is due to increased levels of temperature fluctuations in the flow. Secondly, there is a peak in the r.m.s profiles at all measurement stations. Further, it is observed that the peak gets closer to the wall with increasing y . This location was previously re-

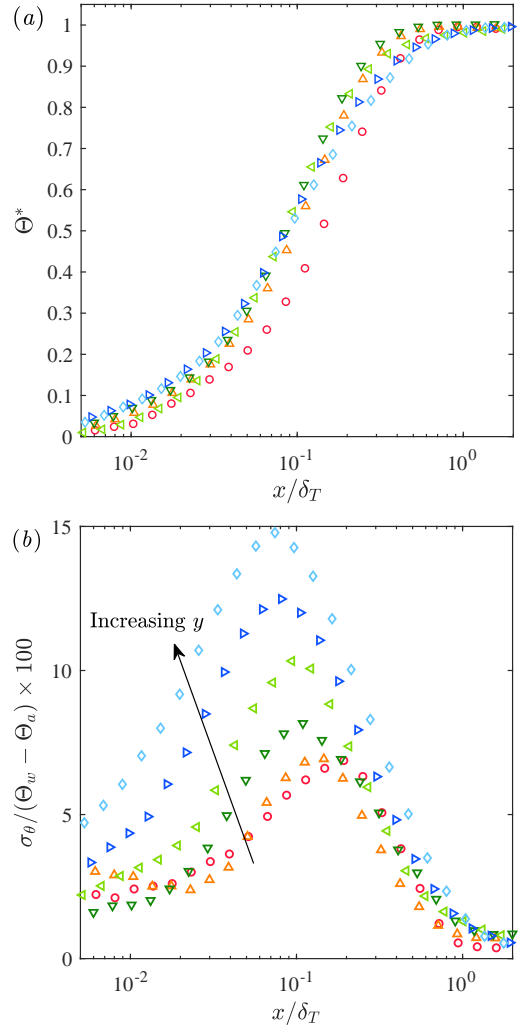


Figure 4: Normalised profiles of (a) mean (Θ^*) and (b) r.m.s (σ_Θ) of temperature as a function of wall-distance (x/δ_T) at six locations along the heated vertical wall.

ported by [7] to coincide with the location of peak turbulence intensity ($xu_\tau/\nu \approx 15$, where u_τ is the friction velocity) in the inner region of a momentum driven velocity boundary layer. Interestingly, [7] found that the characteristics of velocity and temperature fluctuations in natural convection are different, i.e., the locations of maximum velocity and temperature fluctuations are fairly far apart. Finally, it is clear that one length scale is inadequate to collapse the r.m.s profiles of temperature across the entire thermal boundary layer. For instance, in figure 4(b), there is a good collapse of intensity profiles only in the outer region when δ_T is used for normalisation. In contrast, [7] reported collapse of intensity profiles in the inner region (see figure 14 in their paper) when normalised by friction temperature (defined based on heat flux at the wall and friction velocity).

Convection Velocity

In this section, we will make use of simultaneous measurements of temperature fluctuations acquired using three cold wires, which are separated in the y direction as illustrated in the schematic (cf. figure 1(a)). At first, a sample of time series signals of fluctuating temperature from the three probes over a period of 20 seconds is presented in figure 5(a). In this particular instance, there is a high degree of correlation between the three signals. A closer observation reveals that the similar

features are observed in the three signals, however, a time-lag can be seen with increasing y . In order to quantify the time-lag properly, we compute the crosscorrelation coefficient of the signals from any two probes i and j as,

$$R_{ij}(\Delta t) = \frac{\overline{\theta_i(t) \theta_j(t + \Delta t)}}{[\sigma_{\theta_i} \sigma_{\theta_j}]}, \quad i = 1, 2 \text{ and } j = 2, 3. \quad (1)$$

Based on this definition, one can estimate the time-lag that corresponds to the maximum value of R_{ij} , i.e., Δt_{\max} . Using this value, we can determine the convection velocity U_c as $\Delta y_{ij}/\Delta t_{\max}$, where Δy_{ij} is the vertical spacing between probes i and j . This procedure is repeated for all measurement points in the thermal boundary layer and the resulting distribution of U_c is shown in figure 5(b) at the fourth measurement station (similar trend is seen at other locations) for three different power settings of the lamp. It is observed that U_c remains practically constant across the thermal boundary layer. This is possibly due to the correlation being dominated by large-scale thermal structures (or) plumes that fill most part of the boundary layer and travel along the heated wall. For comparison, the results of U_c at different Ra (achieved by changing the heat input) are also presented in figure 5(b). As one would expect, U_c increases with heat input, however, the increase in U_c is not linearly proportionate to the increase of heat input. For this reason, we plotted the values of U_c (averaged across the thermal boundary layer) as a function of Ra using a logarithmic scale for both abscissa and ordinate axes. Interestingly, we find that U_c has a linear trend in this type of representation, indicating that U_c has a power law dependence on Ra . Upon fitting a power law to the data, we found that the exponent is approximately 0.256. Thus, we may be able to express $U_c \propto Ra^{1/4}$.

Conclusion

Experiments are performed in a natural convection boundary layer developing on a vertical heated wall. Statistics of mean temperature revealed that a laminar flow is present in the test rig. Further, it is noted that thermal boundary layer grows as $y^{1/2}$, in agreement with the analytical expression for a laminar flow. A single length scale is found to collapse mean temperature distributions across the entire thermal boundary layer. In contrast, such behaviour is not observed in the r.m.s profiles of temperature fluctuations suggesting separation between inner and outer length scales. Simultaneous measurements of temperature fluctuations at three vertically separated points enabled us to compute the convection velocities of thermal structures. It is observed that U_c is invariant across the laminar thermal boundary layer for constant heat input but changed as $Ra^{1/4}$ when the heat input to the hot wall is varied. As an ongoing investigation, we are currently conducting velocity measurements using hotwire anemometry by taking into account the effect of temperature on velocity. As a long term goal of this study, we wish to expand this experimental campaign to a larger test rig where Rayleigh numbers (10^{11} and higher) can be achieved.

References

- [1] Cheesewright, R., Turbulent natural convection from a vertical plane surface, *J. Heat Transf.*, **90**, 1968, 1–6.
- [2] Nakao, K., Hattori, Y. and Suto, H., Numerical investigation of a spatially developing turbulent natural convection boundary layer along a vertical heated plate, *Int. J. Heat and Fluid Flow*, **63**, 2017, 128–138.
- [3] Patterson, J. C. and Imberger, J., Unsteady natural convection in a rectangular cavity, *J. Fluid Mech.*, **100**, 1980, 65–86.

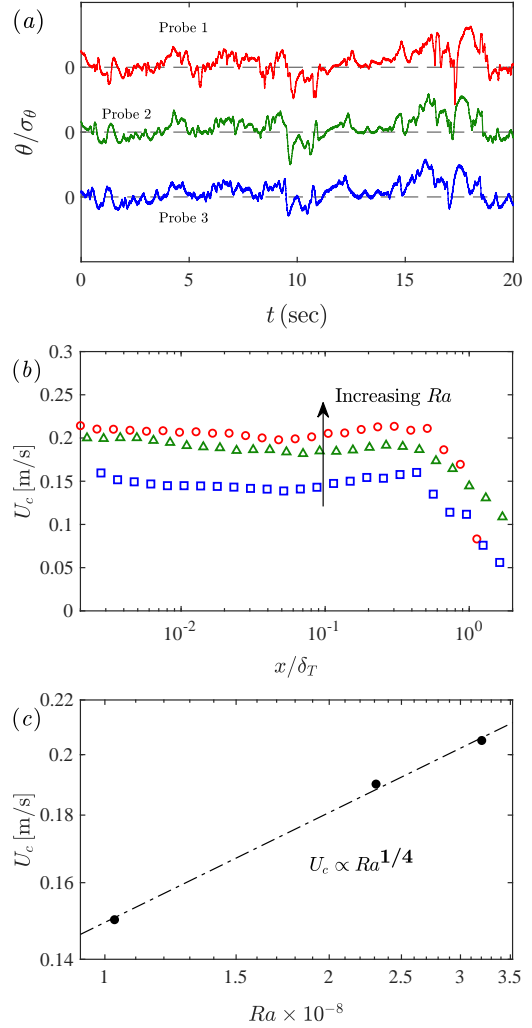


Figure 5: (a) Time series signals of fluctuating temperature over a duration of 20 sec from the three probes. (b) Distributions of convection velocity (U_c) as a function of x/δ_T . (c) U_c vs. Rayleigh number (Ra) on a log-log scale. Note that dot-dashed line is a power-law fit to the experimental data.

- [4] Patterson, J. C., Lei, C., Armfield, S. W. and Lin, W., Scaling of unsteady natural convection boundary layers with a non-instantaneous initiation, *Int. J. Thermal Sci.*, **48**, 2009, 1843–1852.
- [5] Schlichting, H., *Boundary-layer theory*, Springer, 1974.
- [6] Smith, R. R., *Characteristics of turbulence in free convection flow past a vertical plate.*, Ph.D. thesis, 1972.
- [7] Tsuji, T. and Nagano, Y., Characteristics of a turbulent natural convection boundary layer along a vertical flat plate, *Int. J. Heat and Mass Transf.*, **31**, 1988, 1723–1734.
- [8] Tsuji, T. and Nagano, Y., Turbulence measurements in a natural convection boundary layer along a vertical flat plate, *Int. J. Heat and mass Transf.*, **31**, 1988, 2101–2111.
- [9] Vliet, G. C. and Liu, C. K., An experimental study of turbulent natural convection boundary layers, *J. Heat Transf.*, **91**, 1969, 517–531.
- [10] Wells, A. J. and Worster, M. G., A geophysical-scale model of vertical natural convection boundary layers, *J. Fluid Mech.*, **609**, 2008, 111–137.